Finite-Set Model Predictive Decoupled Active and Reactive Power Control for Wind Energy Systems

B. Babes*,[1], A. Bouafassa[2] and A. Boutaghane[1]
[1]Research Center in Industrial Technologies CRTI P.O. Box 64, Cheraga 16014 Algiers, Algeria
[2]Département E.E.A, Ecole Nationale Polytechnique de Constantine, Campus Constantine-3 Constantine, Algérie
E-mail address: elect_babes@yahoo.fr

Keywords

« Maximum power point tracking (MPPT)», « Finite-set model predictive control (FS-MPC)», « Permanent magnet synchronous generator (PMSG)», « Wind energy system».

Abstract

This paper introduces a novel approach for direct power control of three-phase voltage source inverter in grid connected distribution wind energy systems. In this approach, the control of active and reactive power is based on finite-set model predictive control strategy. The proposed strategy has the simplicity of the direct power control technique and doesn't require any current control loops. To meet the future generation of Permanent magnet synchronous generator wind turbines, a DC-DC boost converter is proposed at the machine-side to simplify the control and potentially reduce the cost of the wind energy system. The wind generation system requirements, such as maximum energy harvesting and regulation of grid active and reactive power are expressed as cost functions. Best switching states are selected and applied to the power converters during each sampling interval based on the minimization of cost functions. The feasibility of the proposed configuration and control scheme are verified through dSPACE 1104 experiments on a low power prototype.

I. Introduction

In efficient wind energy generation system, three main research areas play a crucial role: (i) semi-conductor devices, (ii) arrangement of these devices, and (iii) proper turn on/off of these devices. The power converters' control is a very active research topic and is constantly evolving according to the technological developments in semiconductor devices and control platforms, control requirements, power quality standards, and grid code requirements, etc. [1-3]. To design an efficient controller, one needs to know about the true behavior of the plant to be controlled. A power electronic converter exhibits the following properties, constraints and requirements [4, 5]:

- Nonlinear nature.
- Contains finite number of switching states, for example 8 switching states are available for two level three-phase voltage source converter.
- Favors discrete-time implementation using the industry standard digital control plat-forms.

Different predictive strategies have been used in power electronics and drives [4, 6], namely deadbeat control, hysteresis-based predictive control, trajectory-based predictive control and FS-MPC. The FS-MPC strategy has proved one of the best methods for treating all the above properties and conditions. Recent works demonstrated that FS-MPC can easily be applied to a wide range of power converters, drives, and wind energy systems [7]. Compared to the classical control techniques, this scheme eliminates the need for linear PI regulators and the modulation stage, and offers a conceptually different approach to control the power converters. This is truly a model-based optimization control strategy, and involves a large number of calculations [4, 6]. However, the computational issue is not prominent due to the advanced digital control platforms available in the market. It is anticipated that

this will be one of the next generation control tools, and thus is considered in this work as a subject to control the wind energy systems. The rest of this paper is organized as follows: The system under consideration is discussed in section 2, in section 3 the proposed FS-MPC strategy for generator and grid-side converters is explained, Section 4 is related to the experimental results followed by a comments about the performance of the proposed controllers, the paper ends with the conclusions (Section 5).

II. System configuration

The power conversion system for direct-driven PMSG in grid connected distribution generation system is shown in Fig. 1. The system consists of three stages: AC/DC, DC/DC and DC/AC, and these are implemented using a passive diode rectifier, a DC/DC boost converter and three-phase two-level inverter, respectively. The DC/DC boost converter enables MPPT operation for the wind generation system. The system can be operated efficiently in the complete wind speed range by controlling the gating signals for the DC/DC boost converter. The output of DC/DC boost converter directly fits the DC-link capacitor of the grid-tied inverter. This second DC-link provides decoupling for the machine- and grid-side converters. The inverter is used to transfer power from distributed generation system to the utility grid.

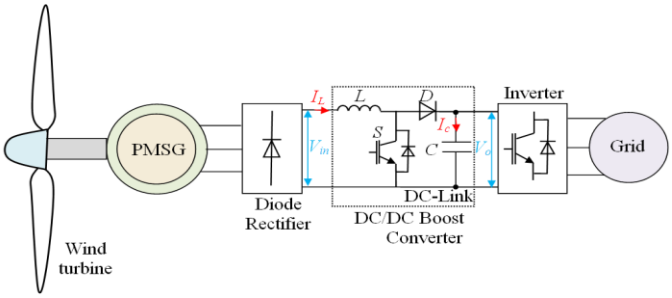

Fig. 1: Considered wind energy system.

II.1 Wind turbine model

The rotating mechanical power of the turbine can be formulated as follows:

$$P_t = 0.5\rho\pi R^2 C_p V_w^3 \tag{1}$$

where ρ is the air density, R is the turbine radius, V_w is the wind velocity, and C_p is the power conversion coefficient. The C_p of a wind turbine is affected by the tip-speed ratio (λ), which is calculated with:

$$TSR = \lambda = \frac{\omega_m R}{V_w} \tag{2}$$

Fig. 2 illustrates the maximum turbine power relates to λ_{opt} and C_{p_max}.

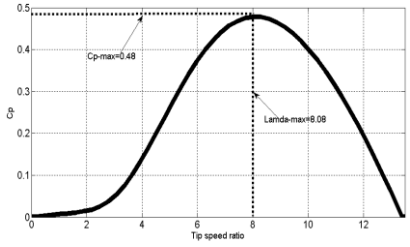

Fig. 2: Power coefficient versus TSR.

The optimum power from a wind turbine can be calculated as follows:

$$P_{m\_opt} = 0.5\rho A C_{p\_\max}\left(\frac{\omega_{m\_opt} R}{\lambda_{opt}}\right)^3 = K_{opt}\left(\omega_{m\_opt}\right)^3 \tag{3}$$

where A is the area swept of a wind turbines blades, ω_{m_opt} is an optimum rotation speed for a specific wind speed, and K_{opt} is an optimum wind constant provided by equation (4):

$$K_{opt} = 0.5\rho AC_{p\_\max}\left(\frac{\omega_{m\_opt}R}{\lambda_{opt}}\right)^3 \quad (4)$$

The optimum torque can be calculated by:

$$T_{m\_opt} = K_{opt}\left(\omega_{m\_opt}\right)^2 \quad (5)$$

II.2 DC/DC boost converter model

A simplified circuit as illustrated in Fig. 3 is derived to simplify the modeling of the DC/DC boost converter.

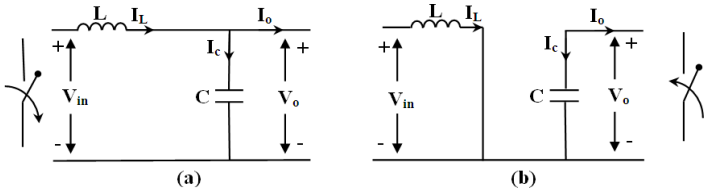

Fig. 3: Functioning modes of the DC/DC boost converter

As illustrated in Fig. 3(a), the switch *S* is in off state (*s*(*t*)=0), and the load is connected to the voltage source (V_{in}). So, the DC/DC boost converter reacts as described by equation (6):

$$\frac{di_L}{dt} = -\frac{1}{L}v_o + \frac{1}{L}v_{in} \quad (6)$$

When switch *S* is in on state (*s*(*t*)=1) as showed in Fig. 3(b), the first-order terms disappear and the former expression system becomes as:

$$\frac{di_L}{dt} = \frac{1}{L}v_{in} \quad (7)$$

II.3 AC/DC Voltage source inverter (VSI) model

The power circuit of the voltage source inverter (VSI) using the electrical scheme is shown in Fig. 4.

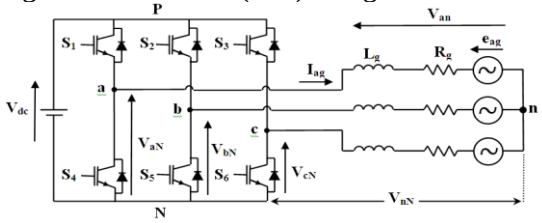

Fig. 4: Voltage source inverter power circuit.

The switching state of the power switches S_n, with n = 1,..., 6, can be described by the switching signal $S_n(t)$ defined as follows:

$$S_n(t) = \begin{cases} 1, \text{ when power switch is "on"} \\ 0, \text{ when power switch is "off "} \end{cases} \quad (8)$$

A switching model for VSI topology may be represented mathematically, such as equation (9):

$$\begin{bmatrix} v_{ab}(t) \\ v_{bc}(t) \\ v_{ac}(t) \end{bmatrix} = \begin{bmatrix} \frac{\{s_1(t)-s_2(t)\}-\{s_3(t)-s_4(t)\}}{2} \\ \frac{\{s_3(t)-s_4(t)\}-\{s_5(t)-s_6(t)\}}{2} \\ \frac{\{s_5(t)-s_6(t)\}-\{s_1(t)-s_2(t)\}}{2} \end{bmatrix} V_{dc} \quad (9)$$

II.4 Grid Model

The grid voltage is modeled as a three-phase balanced voltage sources. The three-phase system can be modeled as three independent, but equivalent, single-phase systems as represented in Fig. 5.

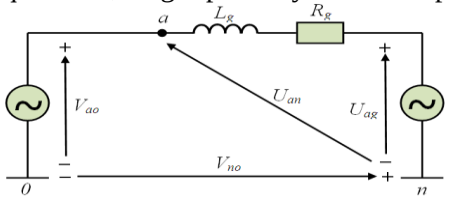

Fig. 5: Equivalent single-phase grid circuit.

The equations for grid current can be rewritten in the α-β coordinates as:

$$U_{\alpha\beta} = L_g \frac{dI_{\alpha\beta}}{dt} + R_g I_{\alpha\beta} + V_{\alpha\beta} \tag{10}$$

Where L_g and R_g are the equivalent series inductance and resistance of grid-side filter. $V_{\alpha\beta}$ is the the inverter voltage, $I_{\alpha\beta}$ is the grid current vector, and $U_{\alpha\beta}$ is the grid voltage vector. The instantaneous active power exchanged with the grid (P_g) is a scalar product between the line grid voltages and currents instantaneous space vectors, whereas the instantaneous reactive power (Q_g) is a vector product between them, and they can be expressed in $\alpha\beta$ coordinates as:

$$P_g = \frac{3}{2}\left(U_\alpha I_\alpha + U_\beta I_\beta\right) \tag{11}$$

$$Q_g = \frac{3}{2}\left(U_\beta I_\alpha - U_\alpha I_\beta\right) \tag{12}$$

The instantaneous change of P_g and Q_g can be obtained from equations (11) and (12) as:

$$\frac{dP_g}{dt} = \frac{3}{2}\left(\frac{dU_\alpha}{dt} I_\alpha + U_\alpha \frac{dI_\alpha}{dt} + \frac{dU_\beta}{dt} I_\beta + U_\beta \frac{dI_\beta}{dt}\right) \tag{13}$$

$$\frac{dQ_g}{dt} = \frac{3}{2}\left(\frac{dU_\beta}{dt} I_\alpha + \frac{dI_\alpha}{dt} U_\beta - \frac{dU_\alpha}{dt} I_\beta - U_\alpha \frac{dI_\beta}{dt}\right) \tag{14}$$

Knowing that the mains voltage is sinusoidal and balanced, the components can be given by the following equation:

$$\overline{U} = U_\alpha + jU_\beta = \left|\overline{U}\right| e^{j\omega t} = \left|\overline{U}\right| \cos\omega t + j\left|\overline{U}\right| \sin\omega t \tag{15}$$

The following equations can be deduced form equation (15) as:

$$\frac{dU_\alpha}{dt} = \frac{d\left(\left|\overline{U}\right| \cos\omega t\right)}{dt} = -\omega\left|\overline{U}\right| \sin\omega t \tag{16}$$

$$\frac{dU_\beta}{dt} = \frac{d\left(\left|\overline{U}\right| \sin\omega t\right)}{dt} = \omega\left|\overline{U}\right| \cos\omega t \tag{17}$$

To simplify, equations (16) and (17) become as:

$$\frac{dU_\alpha}{dt} = -\omega U_\beta \tag{18}$$

$$\frac{dU_\beta}{dt} = \omega U_\alpha \tag{19}$$

Substituting equations (10), (18), and (19) into equations (13) and (14), the power variations can thus be obtained as:

$$\frac{dP_g}{dt} = \frac{3}{2}\left[-\omega U_\beta I_\alpha + \frac{U_\alpha}{L_g}\left(V_\alpha - U_\alpha - I_\alpha R_g\right) + \omega U_\alpha I_\beta + U_\beta\left(V_\beta - U_\beta - I_\beta R_g\right)\right] \tag{20}$$

$$\frac{dQ_g}{dt} = \frac{3}{2}\left[\omega U_\alpha I_\alpha + \frac{U_\beta}{L_g}\left(V_\alpha - U_\alpha - I_\alpha R_g\right) + \omega U_\beta I_\beta - U_\alpha\left(V_\beta - U_\beta - I_\beta R_g\right)\right] \tag{21}$$

By considering equations (11) and (12), $\overline{U}\overline{V}^* = \left(U_\alpha V_\alpha + U_\beta V_\beta\right) + j\left(U_\beta V_\alpha - U_\alpha V_\beta\right)$, and $\left|\overline{U}\right|^2 = U_\alpha^2 + U_\beta^2$, equation (20) and (21) can be rewritten as:

$$\frac{dP_g}{dt} = -\frac{R_g}{L_g} P_g - \omega Q_g + \frac{3}{2L_g}\left(\mathrm{Re}\left(\overline{U}\,\overline{V}^*\right) - \left|\overline{U}\right|^2\right) \tag{22}$$

$$\frac{dQ_g}{dt} = \omega P_g - \frac{R_g}{L_g} Q_g + \frac{3}{2L_g}\mathrm{Im}\left(\overline{U}\,\overline{V}^*\right) \tag{23}$$

III. Control system development

This section presents a control development for a boost converter and a VSI using FS-MPC strategy.

III.1 FS-MPC of DC/DC boost converter with Maximum Power Extraction

III.1.1 MPPT control

The steps required for the MPPT control are as follows:

1. The wind velocity V_w is measured.
2. The desired speed ($\omega^* = \omega_{r\_opt}$) is expressed as:

$$\omega^* = \frac{\lambda_{opt}}{R} V_w \tag{24}$$

3. The error between desired and actual speed is fed into the PI controller to set the reference torque (T_e^*). The reference torque can be calculated as:

$$T_e^* = \left(K_{p\omega} + \frac{K_{i\omega}}{S} \right) (\omega^* - \omega_r) \tag{25}$$

4. The reference torque (T_e*) contributes to determinate the reference rectified current (I_L*) by measuring the rectified voltage (V_{in}), as indicated in the following equation:

$$I_L^* = \frac{T_e^* \omega_r}{V_{in}} \tag{26}$$

5. The I_L^* obtained from equation (26), the actual rectified current I_L, V_{in} and V_o are defined as input variables of the digital FS-MPC to generate control pulses for operating the wind turbine at the optimum speed.

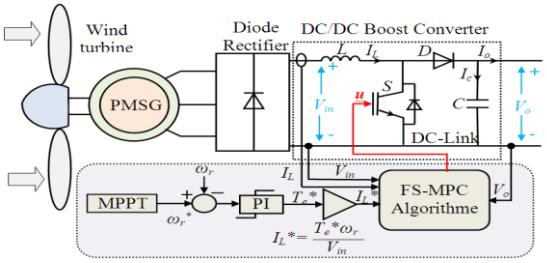

Fig. 6: DC/DC Boost converter control.

III.1.2 Design of FS-MPC for DC/DC boost converter

The aim of FS-MPC of power converters is the use of the converter model to predict the future behavior of the system variables. To predict the future behavior of the controlled variables, the discrete-time model of the boost converter must be established. For simplicity, the forward Euler method is used here. The discrete-time model of the boost converter is used to derive equation (6) and (7), considering the sampling period T_s, when the switch is turned "off" or "on" the predicted control variables is given by equation (27) and (28), respectively.

$$i_L(k+1) = i_L(k) + \frac{T_s}{L}\left(v_{in}(k) - v_o(k)\right) \tag{27}$$

$$i_L(k+1) = i_L(k) + \frac{T_s}{L} v_{in}(k) \tag{28}$$

In our studied case the cost function for the boost converter is given by the following equation:

$$J = \left| i_L(k+1) - i_L^* \right| \tag{29}$$

The cost function guarantees the tracking of the rectified current I_L from the reference current I_L* delivered by the MPPT control. All steps of the proposed FS-MPC algorithm are explained in Fig. 7.

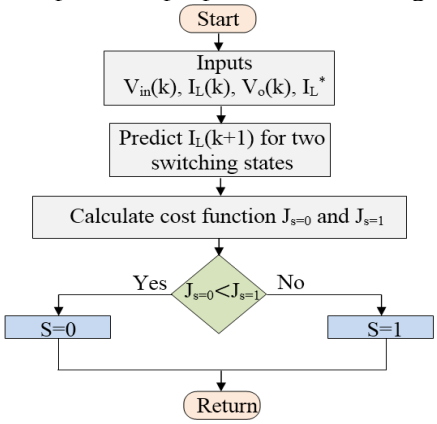

Fig. 7: Flow chart of FS-MPC.

III.2 FS-MPC for direct Power Control of VSI

Various schemes of control systems for the grid-tied inverter were proposed [8]. Presented stable systems are based on decoupled control of the grid power components. Here, to design the structure of the control system a simpler FS-MPC scheme is developed. Such strategy makes it possible to directly control the power of the whole system without inner control loops. In order to independently control the grid power components (P_g and Q_g), the behavior of the grid active and reactive power should be predicted. Prediction equations for the both powers can be defined by discretising equations (30) and (31). Hence, the discrete-time model of the grid power components is as follows:

$$P_g(k+1) = T_s\left[-\frac{R_g}{L_g}P(k) - \omega Q(k) + \frac{3}{2L_g}\left(\mathrm{Re}\left(\overline{UV}^*\right) - \left|\overline{U}\right|^2\right)\right] + P_g(k) \tag{30}$$

$$Q_g(k+1) = T_s\left[\omega P(k) - \frac{R_g}{L_g}Q(k) + \frac{3}{2L_g}\mathrm{Im}\left(\overline{UV}^*\right)\right] + Q_g(k) \tag{31}$$

The next step is to evaluate the effects of each voltage vector on the grid power components and to select the one which produces the least power ripple according to a specific cost function. For this command, the control goals are chosen as the power factor of the AC grid, which can be regulated by controlling the active power (P_g) and reactive power (Q_g).
Consequently, the cost function for 3PH-VSI can be expressed as follows:

$$J = \sqrt{\left(P_g^* - P_g(k+1)\right)^2 - \left(Q_g^* - Q_g(k+1)\right)^2} \tag{32}$$

The block diagram of grid-side inverter control that's the FS-MPC approach performs a direct control of P_g and Q_g for the possible switching combinations is depicted in Fig. 8.

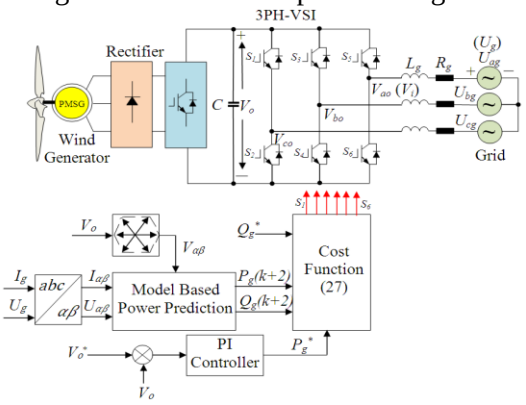

Fig. 8: Proposed FS-MPC direct power control strategy

IV. Experimental results and discussion

An experimental platform of wind energy system is developed in the laboratory as shown in Fig. 9 to verify the performance of the proposed FS-MPC strategy.

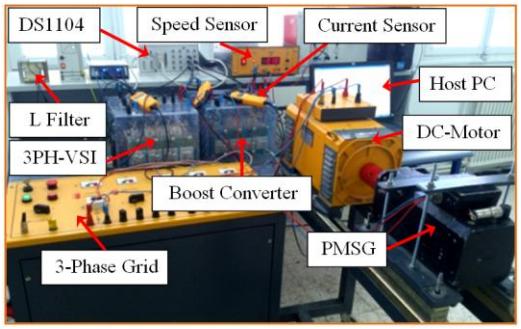

Fig. 9: Prototype of direct-driven wind energy system.

Fig. 10(a)-(j) show experimental results presented using the Control-Desk software. The wind velocity is shown in Fig .10(a). Fig. 10(b) shows that the rotor speed can track the tendency of the optimal reference speed very well and adjust the turbine torque to extract maximum energy from the PMSG. The power coefficient C_p is usually close to the optimal value of C_{p_max}= 0.48 as depicted in Fig. 10(c).

Fig. 10(d) shows the control performance of the rectified current. As depicted, the control performance of the proposed FS-MPC algorithm is very good under wind variations. Fig. 10(e) presents the change in PMSG torque, we can note that its value increases as the wind velocity increases. The mechanical power is illustrated in Fig. 10(f). The DC-link voltage is controlled at its reference with good precision as shown in Fig. 10(g). The grid current controlled by the FS-MPC is presented in Fig. 10(h). The grid current can reach the steady state within one cycle, which demonstrates that the FS-MPC strategy has good dynamic performance. The grid current is in phase with the main voltage, as shown in Fig. 10(i). Fig. 10(j) shows that good tracking performances are attained in terms of grid power.

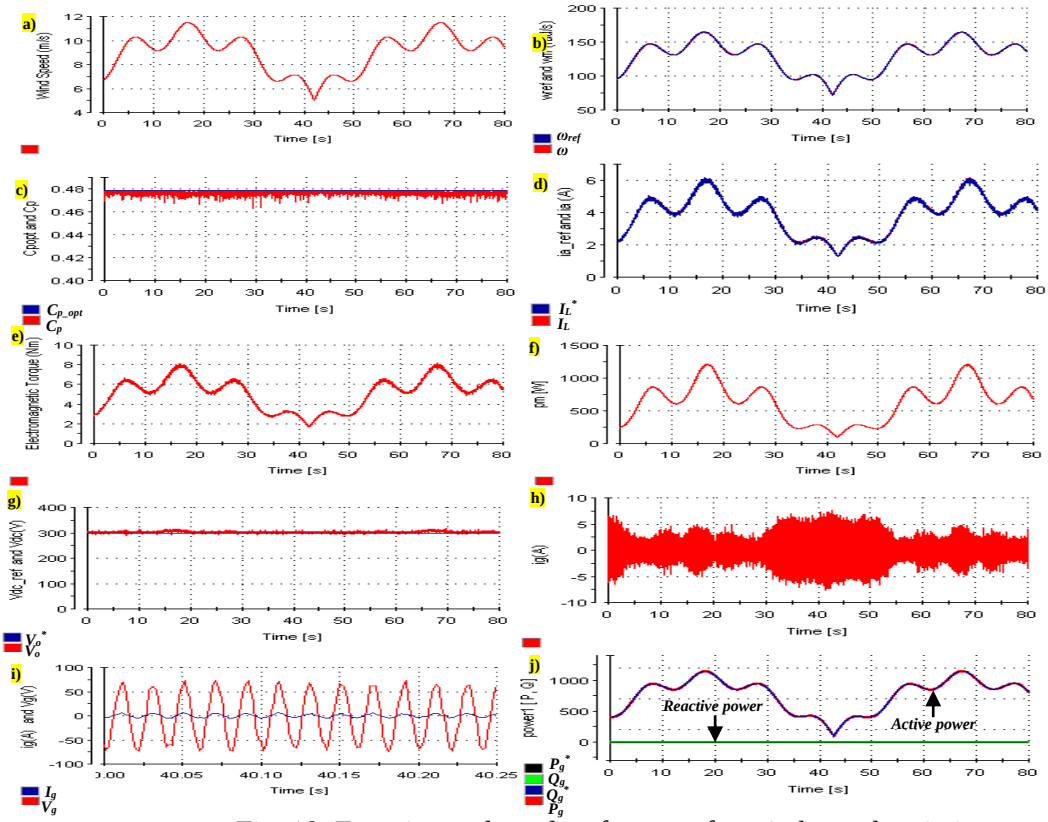

Fig. 10: Experimental results of system for wind speed variation.

The measured results of the grid-interfaced wind energy system under steady-state condition, are illustrated in Fig. 11(a) to 11(d). It is clearly seen from Fig. 11(a) that the total harmonic distortion (THD_i) of the grid current is less than 5% in the whole three-phase. Fig. 11(b) shows the waveforms of the power factor (PF) versus grid power. It is obvious that the PF of utility grid is very close to the unity. Fig. 11(c) shows the three-phase grid currents of sinusoidal waveforms. The DC link voltage (V_o) is conserved close to its references with good precision and stability. The injected current is in phase with the main voltage, as illustred in Fig. 11(d).

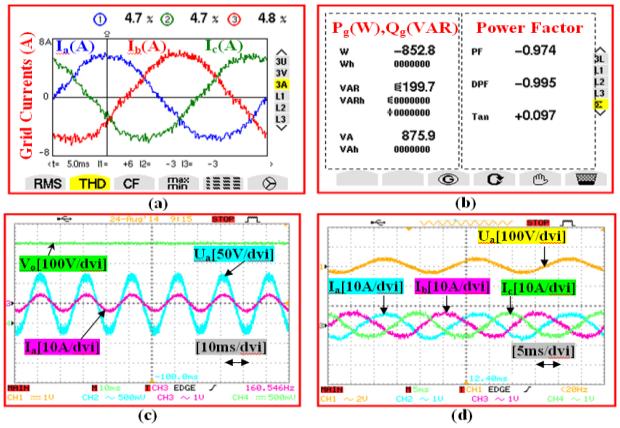

Fig. 11: Steady-state waveforms of proposed FS-MPC direct power control.

The experimental results for unity, lagging, and leading power factor with corresponding grid reactive power are shown in Fig. 12(a) to 12(c), respectively. The first operating with a unity power factor (Fig. 12(a)) and the second one with a lagging and leading PF (Fig. 12(b) and 12(c)) are in phase for the first operation and phase shifted for the second operation. In addition, the reactive power reacts appropriately in both tests.

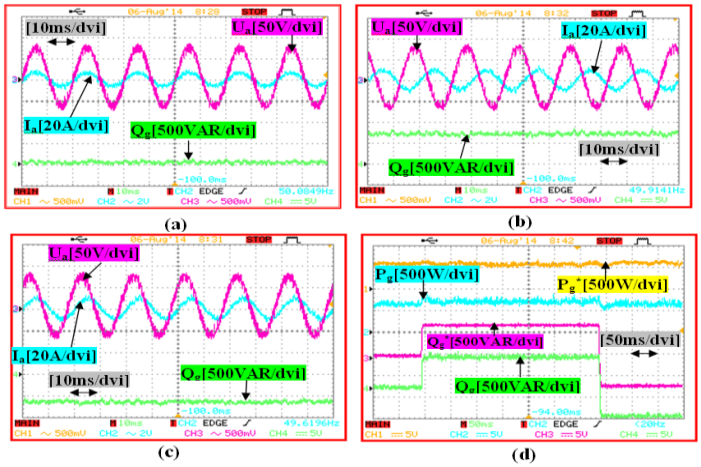

Fig. 12: Steady-state waveforms of FS-MPC direct power control.

Conclusion

In this paper, a simple and intuitive approach that uses the FS-MPC algorithm was developed for a PMSG-based wind energy system. The developed control method ensures the decoupling of active and reactive power for the grid-side converter and guarantees maximum power point tracking (MPPT) for the machine-side converter. The wind turbine requirements, such as MPPT and active and reactive power generation, are modeled as the reference control variables. The machine- and grid-side cost functions are defined to deal with these control objectives. During each sampling interval, the control goals are achieved based on minimization of cost functions. The experimental results showed fast, accurate, and effective responses, and the analysis presented in this paper favors the FS-MPC strategy as the next generation control tool to achieve high performance operation for the wind energy systems. The following future research works are suggested as an extension to the knowledge presented in this paper. The stability issues with the FCS-MPC should be studied by employing different discretization methods and prediction horizons. FCS-MPC algorithm can be also applied on pitch control to reduce the mechanical stress on the drive train and improve the energy conversion efficiency.

References

[1] Liserre M, Cardenas R, Molinas M, and Rodriguez J. Overview of multi-MW wind turbines and wind parks, IEEE Trans. Ind. Electron 2011 Vol 58 no 4, pp. 1081-1095

[2] Blaabjerg F and K. Ma. Future on power electronics for wind turbine systems, IEEE J. Emerging and Selected Topics in Power Electron 2013 Vol 1 no 3, pp. 139-152

[3] Blaabjerg F, Liserre M, and K. Ma. Power electronics converters for wind turbine systems, IEEE Trans. Ind. Appl 2012 Vol 48 no 2, pp. 708-719

[4] Kouro S, Cortes P, Vargas R, Ammann U, and Rodriguez J. Model predictive control-A simple and powerful method to control power converters, IEEE Trans. Ind. Electron 2009 Vol 56 no 6, pp. 1826-1838

[5] Rodriguez J and Cortes P. Predictive Control of Power Converters and Electrical Drives, 1sted. Chichester,UK: IEEE Wiley press 2012

[6] Cortes P, Kazmierkowski M, Kennel R, Quevedo D, and Rodriguez J. Predictive control in power electronics and drives, IEEE Trans. Ind. Elec-tron.2008 Vol 55 no 12, pp. 4312-4324

[7] Rodriguez J, Kazmierkowski M.P, Espinoza J.R, Zanchetta P, Abu-Rub H, Young H.A, and Rojas C.A. State of the art of finite control set model predictive control in power electronics, IEEE Trans. Ind. Informat.2013 Vol 9 no 2, pp.1003-1016

[8] Laks J.H, Pao L.Y, and Wright A.D. Control of wind turbines: Past, present, and future, in 2009 American Control Conference 2009, pp. 2096-2103